Evaluation of adsorption and removal of methylparaben from aqueous solutions using amino-functionalized magnetic nanoparticles as an efficient adsorbent: Optimization and modeling by response surface methodology (RSM)

Farzad Mohammadi[a,b,*], Ali Esrafili[b], Hamid Reza Sobhi[c], Mohammad Behbahani[d], Majid Kermani[b], Esrafil Asgari[b,e], Zeinab Rostami Fasih[f]

[a]*Department of Environmental Health Engineering, School of Public Health, Student Research Committee, Iran University of Medical Sciences, Tehran, Iran, Tel. 0098-2188607963, email: mohammadi_f6382@yahoo.com*
[b]*Department of Environmental Health Engineering, School of Public Health, Iran University of Medical Sciences, Tehran, Iran, email: a_esrafily@yahoo.com*
[c]*Department of Chemistry, Payame Noor University, Tehran, Iran, Tel. 0098-864-4228301, email: h.sobhi@pun.ac.ir*
[d]*Faculty of Engineering, Shohadaye Hoveizeh University of Technology, Dasht-e Azadegan, Susangerd, Iran, email: Tel. 0098-9365683776, email: m.behbahani@shhut.ac.ir,*
[e]*Department of Environmental Health Engineering, School of Public Health, Urmia University of Medical Sciences, Urmia, Iran, email: sasgary@gmail.com*
[f]*Department of Environmental Health Engineering, School of Public Health, Tehran University of Medical Sciences, Tehran, Iran, email: rostamifasihz@yahoo.com*

ABSTRACT

Here in, an efficient amino-modified magnetic nano-adsorbent (Fe_3O_4@SiO_2-NH_2) was applied for the removal of methylparaben (MeP) from aqueous solutions and the removal process was fully optimized by a response surface methodology (RSM). Amino-functionalized magnetic nanoparticles (MNPs) were characterized by FTIR, XRD, SEM and VSM analysis. The Box–Behnken design (BBD) was successfully employed to optimize and determine the influential parameters such as pH (3–11), adsorbent dosage (0.1–1.1 g L^{-1}), reaction time (10–120 min) and solution temperature (25–45°C). The optimal conditions obtained for the adsorption of methylparaben were as follows: temperature, 35°C; pH ≈ 7.0; adsorbent dosage, 1.1 g L^{-1}; and reaction time, 120 min. Under the optimized conditions, the adsorption capacity of 98% was achieved for methylparaben. Additionally, the maximum amount of MeP adsorbed on the nano-adsorbent was determined to be about 75 mg/g. The adsorption isotherms and kinetics were well suited to the Langmuir and pseudo-second-order model, respectively. Finally, it was found out that amino-functionalized magnetic nano-adsorbent is of great potential to remove methylparaben from various aqueous media.

Keywords: Fe_3O_4@SiO_2-NH_2; Methylparaben; Response surface methodology; Adsorption

1. Introduction

The term of PPCPs (pharmaceutical and personal care products) was developed by Daughton and Ternes in 1999 [1]. The population growth and modernization of society with extended consumption habits have led the human beings to use a wide variety of PPCPs. As a result, PPCPs residues are ubiquitous in surface and groundwaters [2]. Parabens, classified as esters of para-hydroxybenzoic acid-compounds (i.e., methylparaben (MeP), ethylparaben (EtP), propylparaben (PrP), isopropylparaben (i-PrP), butylparaben (BuB), isobutylparaben (i-BuP) and benzylparaben (BePB)) have been widely used as antimicrobial preserva-

*Corresponding author.

tive especially in personal care products, pharmaceutical and food stuff [3–5]. Parabens have also been consumed due to a high stability over a wide range of pH, low production costs and relatively safe usage [3,6]. MeP is a short-chain paraben, which is the main ingredient of many products [7]. Some physicochemical characteristics of MeP have been outlined in Table 1. Despite the fact that parabens are considered safe and employed for almost a century, the recent studies have raised a great concern over their use and severe impact on human health. In this regard, a number of reports demonstrated that parabens possess genotoxic or estrogenic compounds that can affect the endocrine system and probably cause breast cancer [6,8,9]. In addition, Darbre et al. [10] reported on the presence of MeP at the highest level corresponding to 62% of the total paraben extracted from the patients' cancerous breast tissues. Although, parabens are biologically degradable and significantly removed in wastewater treatment plants, they always exist at low concentration levels in effluents [11–13]. Containing phenolichydroxyl groups, parabens can easily react with free chlorine and turn into chlorinated by-products. These chlorinated by-products are more stable and toxic than the parent species [14]. Moreover, the presence of parabens and their chlorinated by-products has been confirmed in surface, groundwater and river [13,15–18]. Therefore, it is necessary to remove these estrogenic chemicals from aqueous solutions.

Biological degradation of parabens (MeP, EtP, PrP, BuPandi-BuP) is time-consuming lasting 5 days [19,20]. Up to now, several advanced oxidation processes (AOPs) have been applied for the efficient degradation of parabens, including photocatalysis [21,22], ozonation [23,24], and H_2O_2–UV oxidation [25]. To some extent, all mentioned processes suffer from poor efficiency [3,22].

Due to low concentration of parabens in water, the selection of an effective separation technology remains a great challenge in the removal process. Hence, it is vital to develop a promising technique with an improved capacity for the removal of parabens. Adsorption technology has been regarded as a favorable method for the selection of adsorbent. Amongst the available adsorbents used for the removal of pollutants in water treatment process, magnetic nanoparticles (MNPs) have gained considerable attentions
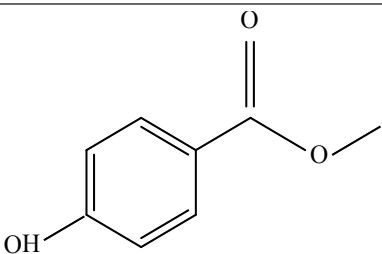
[26]. Iron oxide magnetite (Fe_3O_4) has received a great interest in biomedical applications including drug delivery [27–29], contrast enhancement in magnetic resonance imaging (MRI) as well as the removal of pollutant from the aquatic environment thanks to its large surface-area/volume ratio [30–34]. However, the bare Fe_3O_4 nanoparticles are very reactive and easily oxidized upon direct exposure to specific environments, leading to the reduction in dispersibility and stability. Consequently, the surface of Fe_3O_4 nanoparticles should be modified with a thin silica layer to improve the dispersion due to the chemically inert properties of silica. Silica shell acts as a stabilizer preventing Fe_3O_4 core nanoparticles from oxidization. Furthermore, hydroxyl (–OH) groups on the surface of hydrolysed silica can easily form a covalent bond with the terminal amino group (–NH_2), which could consider ably facilitate its utilization [35–41]. Aminopropyltriethoxysilane (APTES) compound has been found as a promising grafting agent for the surface modification of the silica materials [42–44]. Hence, the present study was centered on the surface modification of MNPs using APTES for the adsorption and removal of MeP from aqueous solutions. To the best of our knowledge, so far this has been the first report on the implementation of APTES for the removal of MeP through adsorption process along with the application of a response surface methodology (Box–Behnken model) for the examination of influential effective operating factors. It should be also highlighted that due to existence of a great number of –NH_2 groups located on the surface of the adsorbent, the efficiency of adsorption is significantly increased. Additionally, the magnetic properties of the mentioned adsorbent highly facilitate its recovery from any aqueous matrices and the potential to be reused for several times.

2. Materials and methods

2.1. Chemicals and materials

Methylparaben (technical reagent grade) was obtained from Sigma-Aldrich Chemical Inc. Ferrous chloride tetrahydrate ($FeCl_2$, $4H_2O$) and ferric chloride hexahydrate ($FeCl_3$, $6H_2O$), were of reagent grade and used without further purification, tetraethylorthosilicate (TEOS), 3-aminopropyl

Table 1
Physical and chemical characteristics of methylparaben

Chemical formula	Chemical structure	Molecular weight (g/mol)	Solubility in water at 25°C (g/100 ml)	pKa	Melting point (°C)	Boiling Point (°C)
$C_8H_8O_3$		152.16[a]	0.25	8.17[b]	131[b]	275[b]

a [3], b [6]

triethoxysilane (APTES) were purchased from Merck, Ltd. Co. (Merck, Darmstadt, Germany).

2.2. Adsorbent preparation

Magnetic Fe_3O_4 nanoparticles were prepared based on a modified co-precipitation method described elsewhere [45, 46]. Fe_3O_4 was prepared with a stoichiometric ratio of 2:1 (Fe^{3+}/Fe^{2+}). Briefly, 11.4 g ferric oxide ($FeCl_3 \cdot 6H_2O$)and 4.1 g ferrous oxide ($FeCl_2 \cdot 4H_2O$) were dissolved in deionized water under the conditions of nitrogen atmosphere, 80°C and vigorous stirring. Afterward, 30 mL NH_4OH (25–30%, w/w) was added dropwise to the solution and stirred for 24 h. Subsequently, the black precipitate was aggregated by a magnetic field, and the residual solution was removed. Finally, the black magnetic Fe_3O_4 nanoparticles were rinsed three times with deionized water and ethanol followed by drying at 50°C under vacuum for 4 h.

For preparation of $Fe_3O_4@SiO_2$, as-prepared magnetic nanoparticles (Fe_3O_4 1.0 g) were diluted in a mixture of 40 mL ethanol and 10 mL deionized water using an ultrasonic water bath for 30 min. For modification, the resulting suspension was added with 0.5 mL TEOS and 2 mL ammonia solution (NH_4OH 25%), and the mixture was stirred at 50°C for 6 h. [47, 48]. In the next step, 1.0 g of the produced $Fe_3O_4@SiO_2$ nanoparticles was diluted in a flask with 25 mL mix of toluene:methanol (1:1, v/v) and ultrasonically dispersed for 15 min. Finally, 2 mL APTES was introduced to the flask while stirring for 4 h. The product was washed with ethanol several times and then dried at 60°C under vacuum for 12 to obtain $Fe_3O_4@SiO_2$-NH_2 [49,50]. Fig. 1 illustrates a schematic representation of the synthesis of the adsorbent used for the removal of MeP.

2.3. Experimental procedures

Prior to initial experiments, various dosages (0.1, 0.6, and 1.1 g/L) of the adsorbent were prepared. All experiments were conducted with RSM. Each 250 mL flask was filled up with the known amounts of MeP and nano-adsorbent to obtain the desirable respective concentrations. The pH of the solution was adjusted to 3, 7 and 11 using 0.1 M H_2SO_4 or NaOH. In addition, the temperature of the solution was adjusted in the range of 25–45°C. The bottles were capped with Teflon-lined screw caps to minimize any loss arising from volatilization. They were then shaken using a thermostatic shaker at 200 rpm under a certain period of time (10, 65 and 120 min). After the time elapsed, a 10 mL aliquot of the sample was pipetted out and the adsorbent was magnetically separated. Finally, the residual concentrations of MeP in the solution were measured by HPLC. Based on the amount of MeP adsorbed, q_e (mg/g) was calculated using Eq. (1):

$$q_e = \frac{V(C_0 - C_e)}{M} \times 100 \tag{1}$$

where C_0 and C_e are the initial and the equilibrium amount of MeP concentration (mg/ L), V, the volume of MeP solution (L), and M is the mass of adsorbent (g). The amount of MeP adsorbed (%) on the adsorbent was determined using the following equation:

$$Adsorption\% = \frac{C_0 - C_e}{C_e} \times 100 \tag{2}$$

2.4. Adsorption equilibrium isotherm of MeP on the nano-adsorbent

The frequently applied adsorption isotherm models namely, the Langmuir and Freundlich models were tested. The Langmuir isotherm is originally based on the assumption that the adsorption occurs in a homogeneous monolayer coverage over an adsorbent surface given by Eq. (3) [51]. Whereas, the Freundlich is an empirical equation [Eq. (4)] that describes the adsorption process taking place on heterogeneous or multilayer surfaces [52].

$$C_e/q_e = 1/K_l q_m + C_e/q_m \tag{3}$$

$$ln q_e = ln k_f + (1/n) \ln C_e \tag{4}$$

where C_e is the equilibrium concentration of the MeP in the solution (mg/L), q_m is the maximum amount of MeP per
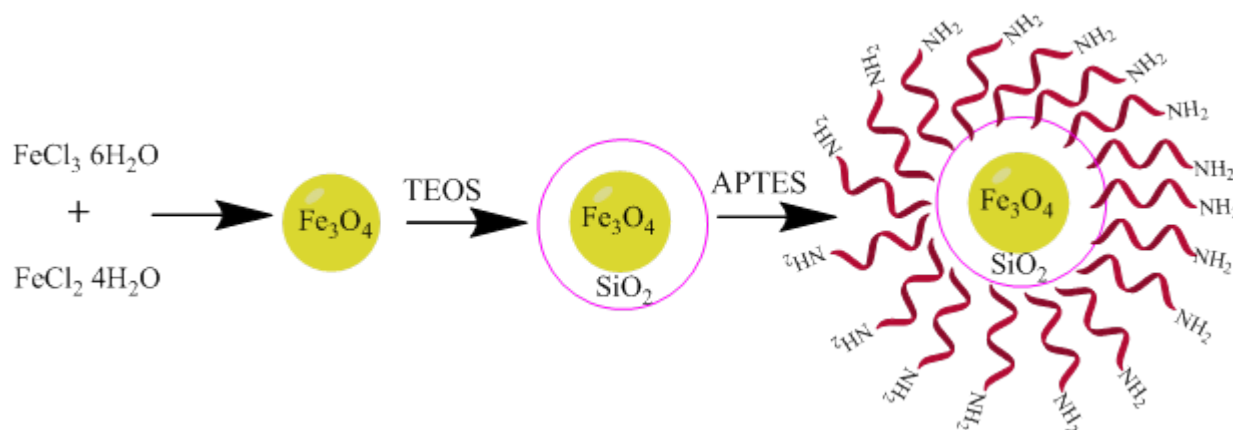

Fig. 1. Synthesis procedure of the $Fe_3O_4@SiO_2$-NH_2 magnetic nano-adsorbent.

unit mass of the adsorbent (mg/g) and k_1 is the Langmuir adsorption constant (mg/L). k_f (mg/g)(L/mg)$^{1/n}$ and n are the constant values relating to the adsorption capacity of the adsorbent and intensity of the Freundlich model, respectively.

2.5. Kinetics of adsorption

The kinetics of MeP adsorption can be analyzed by two kinetic models; the Lagergren pseudo-first-order [Eq. (5)] [53], and pseudo-second-order model based on the adsorption capacity represented by Eq. (6) [54].

$$\ln(q_e - q_t) = \ln q_e - k_e t \qquad (5)$$

$$\frac{t}{q_t} = \frac{1}{k_f} \cdot q e^2 + \frac{t}{q_e} \qquad (6)$$

where q_t (mg/g) is the amount of MeP adsorbed at a given time and q_e (mg/g) is the amount of MeP at equilibrium condition, respectively. k_e (1/min) and k_f (g/mg·min) are the rate constants relating to the first and second order adsorption, respectively.

2.6. Analytical method

As previously mentioned, the concentration of MeP was measured by HPLC (CECIL 4100, USA,waters Alliance 2695 XC with UV–Vis Diode Array detector). Separation of MeP was made on a Nucleodur Sphinx RP column (25.0 cm × 4.6 mm, MZ-1 PerfectSil, Germany) at a flow-rate of 1 ml/min. The mobile phase consisted of a solvent A (water) and B (methanol). A 20-min gradient elution program of A: B/50:50 was employed for the separation. The detection resulted in a well-defined peak for MeP (RT 18 min, 230 nm).

2.7. Processing of variables by Box-Behnken design

RSM based on the Box-Behnken design is one of the most powerful and efficient statistical and mathematical methods applied for evaluating the effect of independent variables on the response function, which can improve and optimize complex procedures [55,56]. Recently, the Box–Behnken design because of practicability and efficiency has been widely implemented by many researchers in various studies (46) [57–60]. In the present study, a 4-factor/3-level-Box–Behnken experimental design was implemented as fol-

Table 2
Independent variables and their respective experimental levels

Variables	Symbol	Level of value		
		−1	0	+1
MNPs dose (g/l)	A	0.1	0.6	1.1
pH	B	3	7	11
Temperature (°C)	C	25	35	45
Time (min)	D	10	65	120

lows: MNPs dosage (A), pH (B), Temperature (C) and Time (D). Each factor at three levels was considered in order to achieve the maximum adsorption efficiency for MeP using the nano-adsorbent. As illustrated in Table 2, the actual variable values were coded as low (–1), center (0) and high (+1). It is also noted that a trial version Design expert 10.0.4.0 (Stat-Ease, 2011) statistical software was used. A total number of experiments ($n = 29$) was set including three replications at the center point to estimate a pure error of sum of squares(see Table 3).

3. Results and discussion

3.1. Characterization of the adsorbent

The surface morphologies of Fe_3O_4 and the adsorbent were initially examined by SEM method as illustrated in Figs. 2A and B. As can be seen,the distribution of amino-functionalized silica over the surface of Fe_3O_4 MNPs is clearly exhibited. This result shows that the surface of Fe_3O_4 MNPs was successfully covered with silica. Besides, the XRD patterns of the synthesized sorbent is illustrated in Fig. 3. The spectra of Fe_3O_4, $Fe_3O_4@SiO_2$ and $Fe_3O_4@SiO_2\text{-}NH_2$ exhibit six distinct peaks with 2Θ at 30.32°, 35.62°, 43.35°, 57.33°, and 62.89° illustrating a cubic spinal structure of the adsorbent [61]. It can be clearly observed from Fig. 3 that the SiO_2 shell and amino groups were uniformly coated on Fe_3O_4 core. Additionally, the successful coating of the SiO_2 shell and amino group on the surface of Fe_3O_4 cores were confirmed by FT-IR experiments performed in the range of 500–4000 1/cm (Fig. 4). As shown in Fig. 4, the bands at 570 cm^{-1} are indicative of the presence of the Fe-O-Fe bond [62]. The Fe-O-Fe bond found in $Fe_3O_4@SiO_2$ and $Fe_3O_4@SiO_2@NH_2$ proved that Fe_3O_4 was embedded in these materials. Furthermore, for $Fe_3O_4@SiO_2$ and $Fe_3O_4@SiO_2\text{-}NH_2$, the peaks at ~1150 cm^{-1} represent the vibration of Si-O-Si bonding [63]. The peak at ~1420 is also assigned to the N-H stretching. As can be concluded, the FT-IR spectroscopy analysis verified the formation of amino groups on silica-coated magnetite nanoparticles [64]. In addition, the VSM magnetization curves of Fe_3O_4, $Fe_3O_4@SiO_2$, and $Fe_3O_4@SiO_2\text{-}NH_2$ nanoparticles are depicted in Fig. 5. The saturated magnetization values of the particles were reduced from 68.5 to 42.2 emu/g (for Fe_3O_4 and for $Fe_3O_4@SiO_2\text{-}NH_2$ MNPs, respectively). These results also reveal that the adsorbent exhibits an excellent magnetic response to a magnetic field. Therefore, the adsorbent is easily and rapidly separated due to a significantly magnetic sensitivity. Note that the reported value is a bit smaller than the magnetization value of the amino-functionalized $Fe_3O_4@SiO_2\text{-}NH_2$ (45.93 emu/g) reported by other researchers[65].

### 3.2. The Box–Behnken design for MeP removal rate and statistical analysis

Results obtained by performing the batch adsorption experiments according to the RSM matrix are summarized in Table 4. The final equation of the quadratic model relating to the experimental results for the MeP adsorption in terms of actual (natural) factors is given below:

Table 3
The Box-Behnken design experiment for four variables and their corresponding responses

Run	A:MNPs (g/L)	B:pH	C:Temperature (°C)	D:Time (min)	Adsorption (%)
1	0.10	7.0	25.00	65.00	27
2	0.60	11.0	45.00	65.00	58
3	1.10	7.0	35.00	120.00	98
4	0.10	3.0	35.00	65.00	21
5	1.10	3.0	35.00	65.00	57
6	0.10	11.0	35.00	65.00	23
7	0.60	7.0	45.00	120.00	88
8	0.10	7.0	45.00	65.00	31
9	0.60	11.0	35.00	120.00	70
10	0.60	7.0	35.00	65.00	54
11	0.60	7.0	35.00	65.00	57
12	1.10	7.0	35.00	10.00	40
13	0.60	3.0	25.00	65.00	47
14	0.10	7.0	35.00	10.00	10
15	1.10	11.0	35.00	65.00	63
16	0.60	7.0	25.00	120.00	77
17	1.10	7.0	25.00	65.00	73
18	1.10	7.0	45.00	65.00	85
19	0.60	3.0	45.00	65.00	45
20	0.60	3.0	35.00	10.00	20
21	0.60	7.0	45.00	10.00	33
22	0.60	7.0	35.00	65.00	56
23	0.60	11.0	35.00	10.00	24
24	0.60	7.0	35.00	65.00	55
25	0.60	7.0	25.00	10.00	30
26	0.10	7.0	35.00	120.00	35
27	0.60	3.0	35.00	120.00	60
28	0.60	11.0	25.00	65.00	53
29	0.60	7.0	35.00	65.00	60
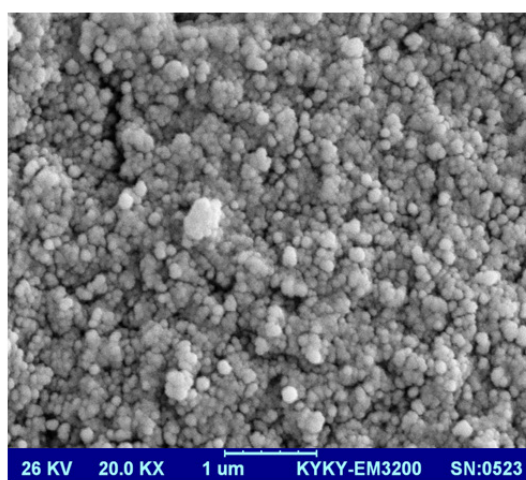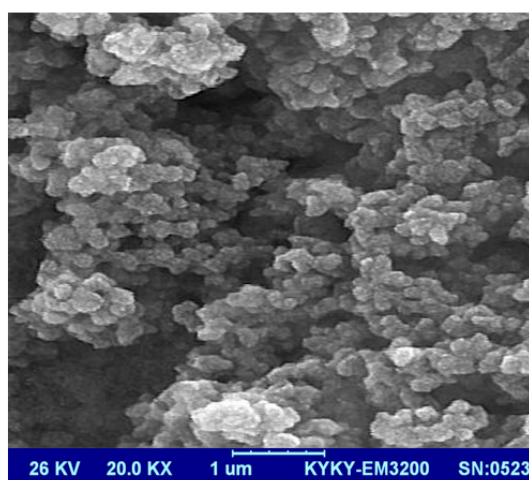
Fe₃O₄　　　　　　　　　　　**Fe₃O₄@SiO₂@NH₂**

Fig. 2. SEM images of Fe_3O_4 (A) and Fe_3O_4@SiO_2-NH_2 (B).
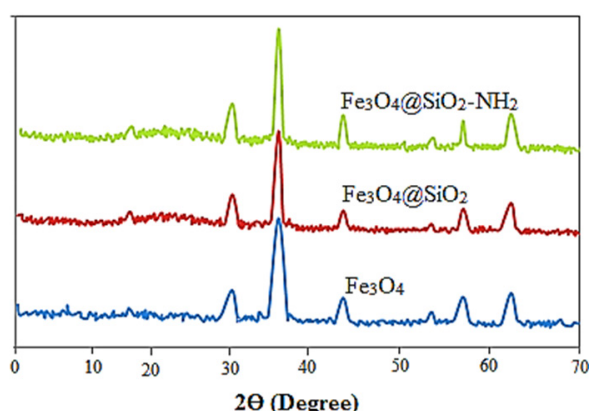
Fig. 3. X-ray diffraction (XRD) spectra patterns of Fe_3O_4, $Fe_3O_4@SiO_2$, and $Fe_3O_4@SiO_2-NH_2$.
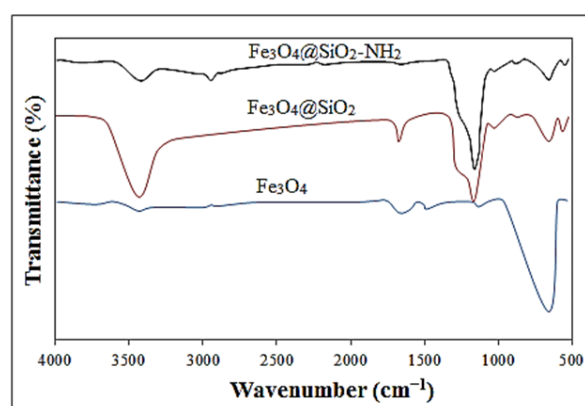
Fig. 4. FT-IR spectra Fe_3O_4, $Fe_3O_4@SiO_2$, and $Fe_3O_4@SiO_2-NH_2$.
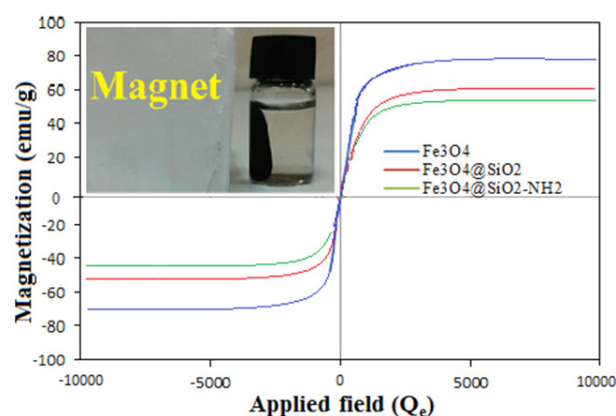
Fig. 5. VSM magnetization curves of Fe_3O_4, $Fe_3O_4@SiO_2$ and $Fe_3O_4@SiO_2-NH2$ at room temperature.

Adsorption = 37.73 + 38.99 A + 6.67 B – 3.31 C + 0.22 D + 0.5 AB + 0.4 AC + 0.3 AD + 0.04 BC + 0.007 BD + 0.004 CD – 25.97 A2 – 0.58 B2 + 0.04 C2 – 0.001 D2 (7)

ANOVA is a suitable statistical technique for the analysis of the statistical significance of the response sur-face quadratic regression model. The significance of the quadratic model was analyzed by F, P and the correlation coefficient value, and the corresponding results of ANOVA are presented in Table 4. The F-value of 71.74 and p-value with a low probability (<0.0001) implied that the quadratic model satisfactorily explained the MeP adsorption on the adsorbent. It is obvious that the value of lack of fit (3.21) is insignificant, which demonstrates the validity of the quadratic model for the MeP adsorption on the adsorbent. The value of determination of correlation coefficient (R^2 = 0.9863) in the present study describes that the regression model is well fitted to the prediction of the performance of the MeP adsorption on the adsorbent. Meanwhile, the value of the predicted determination of coefficient (R^2 = 0.9613) is in agreement with the value of R^2_{adj} = 0.9725. As shown in Table 4, all the p-values of A, B, C, D, AD, A^2, B^2 C^2 and D^2 are less than 0.05, which implies that these variables are highly significant and play an important role in the MeP adsorption efficiency. As can be seen in Fig. 6a, the fitted quality of Eq. (7) was also observed by comparing the MeP adsorption efficiency between the experimental and predicted models. It is expressed that the prediction residuals for the most of the response values were less than 10% and the predicted values are close to the actual results, supporting the fact that the regression model exhibits excellent performance for the MeP adsorption on the adsorbent. To evaluate the model adequacy the normal probability versus studentized residual plot, a graphical diagram for determining residual normality,was drawn [66,67]. As can be seen in Fig. 6b all the graphical residual points on the plot were well distributed (i.e., closely positioned to the straight line), confirming that the model was sufficient to predict the MeP adsorption on the adsorbent. On the whole, it can be concluded that the RSM used in present study was determined to be suitable for the prediction of the MeP adsorption process.

3.3. Model interpretation with three-dimensional plots

3-dimensional response surface plots are the analytical graphs demonstrating the simultaneous mutual interactive effects of two independent variables on the reaction process while keeping another variable at a fixed level [68]. The 3-dimensional surface response plots and their interactive effects of the variable combination on MeP adsorption are shown in Figs. 7a–e. The change in pH value, is likely to be the most important parameter in the adsorption efficiency mainly due to its impact on a) the solubility of the ionic form, b) the concentration of the opposite ions attached to the amino group (–NH_2) of the nano-adsorbent and c) the ionization properties of the nano-adsorbent surface [43]. The evaluation of the effect of pH as the most significant variable is depicted in Figs. 7a, b and f. As shown, the MeP adsorption efficiency was initially enhanced as pH values increased from 3.0 to 7.0 and then gradually decreased within the range of 7.0–11.0. The phenomena could be attributed to the different interactions between the adsorption sites and MeP under a various pH range and to the hydrogen bonding interactions between N and H of the amino group and –OH or –$COOCH_3$ in MeP molecule [69]. In addition, other driving forces such as the

Table 4
Analysis of variance (ANOVA) results for the response surface quadratic model

Source	Sum of squares	df	Mean square	F Value	p-value	Prob > F
Model	13740.47	14	981.46	71.74	< 0.0001	significant
A-MNPs	6030.08	1	6030.08	440.76	< 0.0001	
B-pH	140.08	1	140.08	10.24	0.0064	
C-Temperature	90.75	1	90.75	6.63	0.0220	
D-Time	6120.08	1	6120.08	447.34	< 0.0001	
AB	4.00	1	4.00	0.29	0.5972	
AC	16.00	1	16.00	1.17	0.2978	
AD	272.25	1	272.25	19.90	0.0005	
BC	12.25	1	12.25	0.90	0.3601	
BD	9.00	1	9.00	0.66	0.4309	
CD	16.00	1	16.00	1.17	0.2978	
A^2	273.35	1	273.35	19.98	0.0005	
B^2	554.00	1	554.00	40.49	< 0.0001	
C^2	104.22	1	104.22	7.62	0.0153	
D^2	90.81	1	90.81	6.64	0.0220	
Residual	191.53	14	13.68			
Lack of Fit	170.33	10	17.03	3.21	0.1359	not significant
Pure Error	21.20	4	5.30			
Cor Total	13932.00	28				

R-Squared = 0.9863, Adj R-Squared = 0.9725, Pred R-Squared = 0.9272, Adeq Precision=33.833.
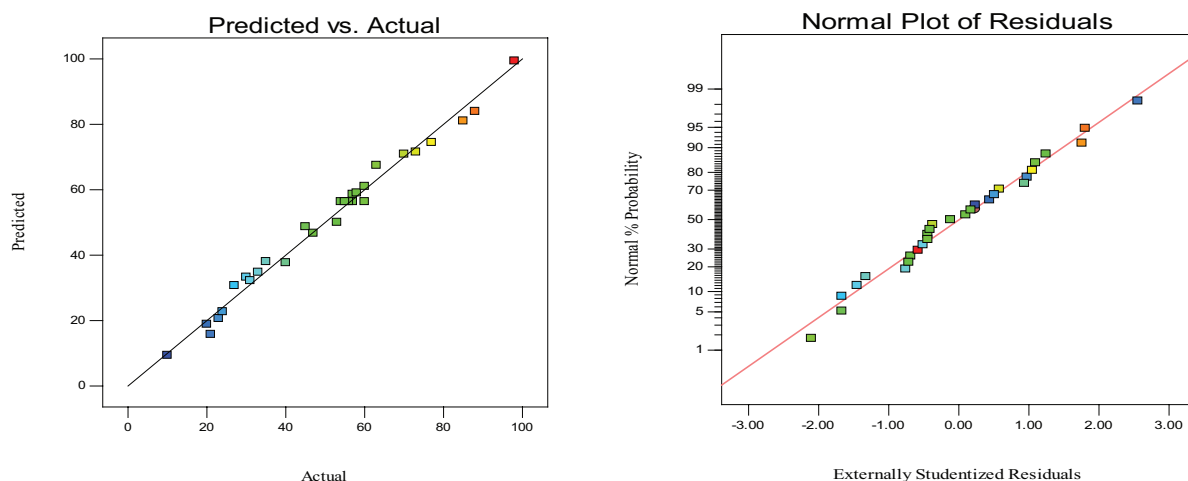

Fig. 6. Comparison of the predicted versus actual (a) and normal probability versus residuals plot (b) for the MeP adsorption on the Fe_3O_4@SiO_2-NH_2 MNPs.

electrostatic interaction between the positively-charged aminopropyl and MeP molecule may play an important role in promoting the MeP adsorption.

According to the study by Wang et al., the optimum pH value for the adsorption of tannic acid on the adsorbent was determined to be 6 [33]. The same group also reported that at pH = 3 the adsorption rate was low, which is probably due to the formation of –NH_3^+ leading to the reduction of MeP adsorption [70]. In fact,at low pH, the adsorbent surface is mainly covered with H_3O^+ ions resulting in the loss of MeP adsorption [71]. This is in agreement with the result

reported in the literature echoing the fact that the neutral pH (pH = 7) is favorite for the adsorption [72].

According to Table 1, at pH ≥ pKa, the ionized form of MeP is predominant; while at pH ≤ pKa, the molecular form will be the major form in the aqueous solution. Consequently, as pH increases, both the adsorbent surface and MeP molecule become more and more negatively charged, leading to an electrostatic repulsion in consequent with a great loss of the MeP adsorption [73].

In a further development, the MeP uptake capacity increased when the adsorbent dosage increased from 0.1 to
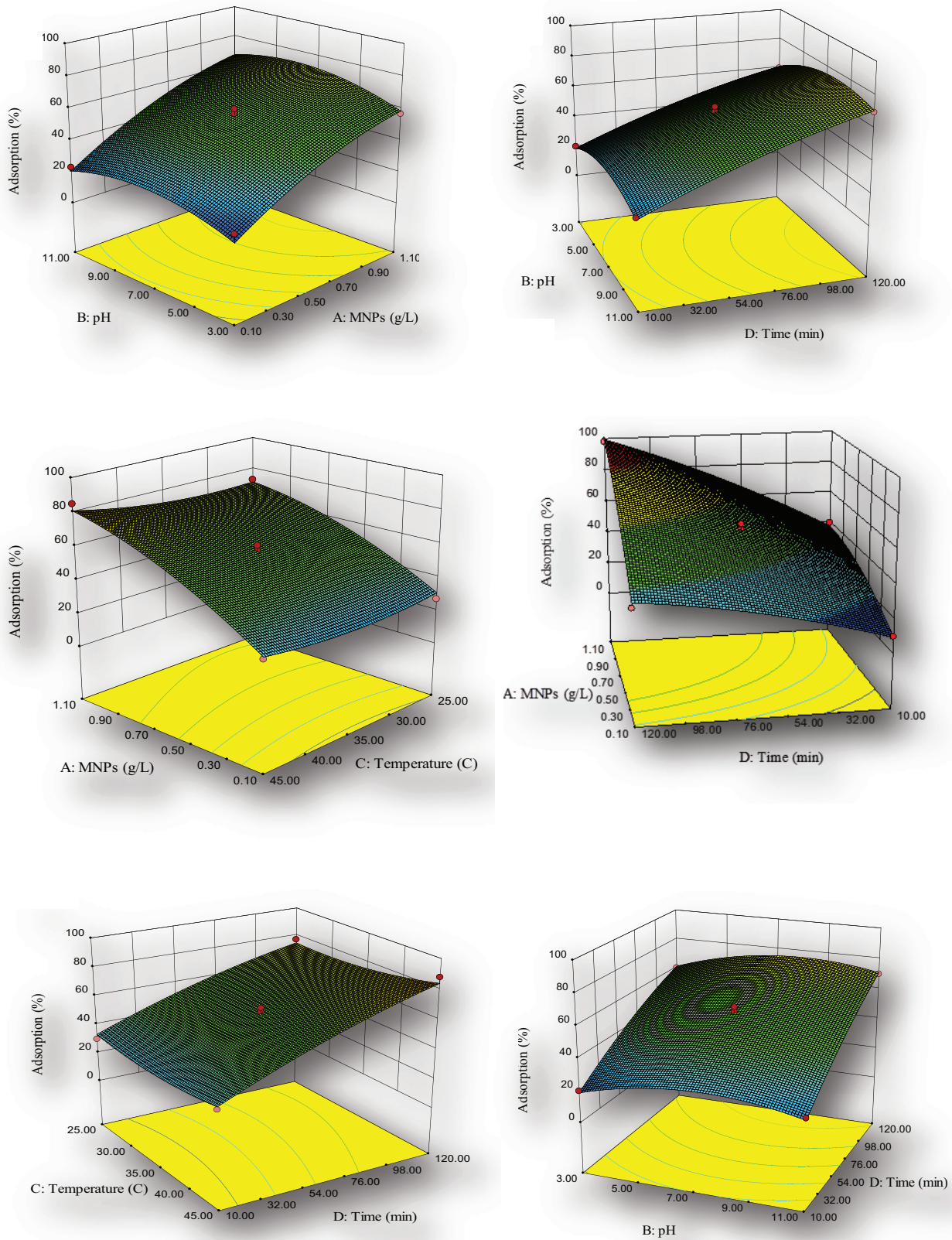
Fig. 7. 3-D plots for the interaction effects of (a) Fe$_3$O$_4$@SiO$_2$-NH$_2$ MNPs dosage and pH, (b) Time and pH (c) Fe$_3$O$_4$@SiO$_2$-NH$_2$ MNPs dosage and Temperature, (d) Time and Fe$_3$O$_4$@SiO$_2$-NH$_2$ MNPs dosage, (e) Temperature and Time, and (F) Time and pH on the removal percentage of MeP using the Fe$_3$O$_4$@SiO$_2$-NH$_2$ MNPs.

1.1 g/ L as illustrated in Figs. 7a, c and d. It is clear that the implication of higher dosages of the adsorbent leads to an increase in the surface area as well as the availability of more affinity binding sites on the adsorbent [74].

The MeP adsorption on the adsorbent was also conducted at different contact time ranging from 10 to 120 min (Figs. 7b and d). It can be seen from the response surface graphs that the MeP adsorption efficiency is enhanced with increasing the contact time from 10 to 120 min. This can be explained by the fact that the adsorbent with a huge number of abundant activated sites could provide sufficient adsorption sites for MeP [75].

Figs. 7c, e, illustrate the adsorption efficiency of MeP on the adsorbent at different temperatures. It can be observed that the adsorption capacity of MeP was enhanced with increasing the temperature from 25 to 45°C, and the maximum adsorption efficiency was obtained at 45°C. Therefore, the adsorption process is of endothermic nature. Similar results were reported by Zhang et al. centering on Pb (II) removal from the aqueous solution using the adsorbent [76].

3.4. Optimization process for MeP adsorption

In order to determine the optimum value for the MeP maximum adsorption efficiency a multiple response method was carried out and the results are tabulated in Table 4. In the Design Expert software, for numerical optimization the possible goals are as follows: minimize, maximize, target, within in range, set to an exact value (factors only) and none (for responses only). Under the optimal conditions designed by the Design Expert software, the favorite objectives for each evaluated parameter (i.e. adsorption time, the nano-adsorbent dosage, pH, and temperature) were selected within the respective range. The response (maximum adsorption of MeP (%)) was defined to obtain the highest efficiency of adsorption rate. To test the optimization values obtained by the Box–Behnken design, the results were experimentally checked and tabulated in Table 5. As can be seen, the additional experimental result was in good agreement with the expected response value, which implies that the Box–Behnken design desirability functions could successfully be applied for the optimization of the adsorption parameters regarding the removal of MeP.

3.5. Kinetics of adsorption

Kinetics of adsorption was conducted under the conditions as follows: different contact times (5, 15, 30, 60, 90, and 120 min), a fixed dosage of the adsorbent (0.6 g/L), MeP concentration (20 mg/L), pH = 7 and temperature of 25°C. The experimental results are summarized in Table 6. It can be observed that the pseudo-first-order model provided the poor kinetic data for MeP uptake on the adsorbent. However, the pseudo-second-order model was well fitted to the correlation coefficient values ($R^2 > 0.99$). Additionally, the experiment q_e (exp) (31.13 mg/g for MeP) and calculated q_e (cal) (32.57 mg/g for MeP) were close to each other.

On the whole, according to the Table 5 the R^2 values (>0.99), it is concluded that the pseudo-second-order was found to be the optimum kinetic model to describe the adsorption of MeP using the adsorbent.

3.6. Adsorption isotherms

The schematic mechanism for the adsorption of MeP on the adsorbent is illustrated in Fig. 8 and all the model parameters and their multiple regression coefficients (R^2) obtained from the two static isotherm models are also tabulated in Table 7 (The applied condition for the experiment was: pH of 7.0, adsorbent dosage of 0.6 g L^{-1} and adsorption time of 120 min). The maximum amount of MeP adsorbed on the adsorbent was determined to be about 75 mg/g. To further clarify the mechanism of MeP adsorption, a number of batch tests were carried out to study the Freundlich and Langmuir isotherm models. As can be seen from Table 7, R^2 values of 0.98 and > 0.99 for the Freundlich and Langmuir isotherm models were obtained at different temperatures, respectively. Accordingly, the experimental data were well fitted to the Langmuir model. This result also suggests that the MeP uptake on the adsorbent follows the monolayer pattern.

3.7. Thermodynamics

To study the thermodynamics of MeP adsorption, a single experiment was carried out at different temperatures (25, 35 and 45°C). Three thermodynamic parameters

Table 5
Optimization results regarding the maximum adsorption efficiency of MeP

Number	Adsorption dose (g/L)	pH	Time (min)	Temperature (°C)	Adsorption rate %
1	1.1	7	120	35	99.4
Add. Exp[a]	1.1	7	120	35	98

[a]Additional experiment

Table 6
The simulated parameters of the kinetic model for the adsorption of MeP on the Fe_3O_4@SiO_2-NH_2 MNPs

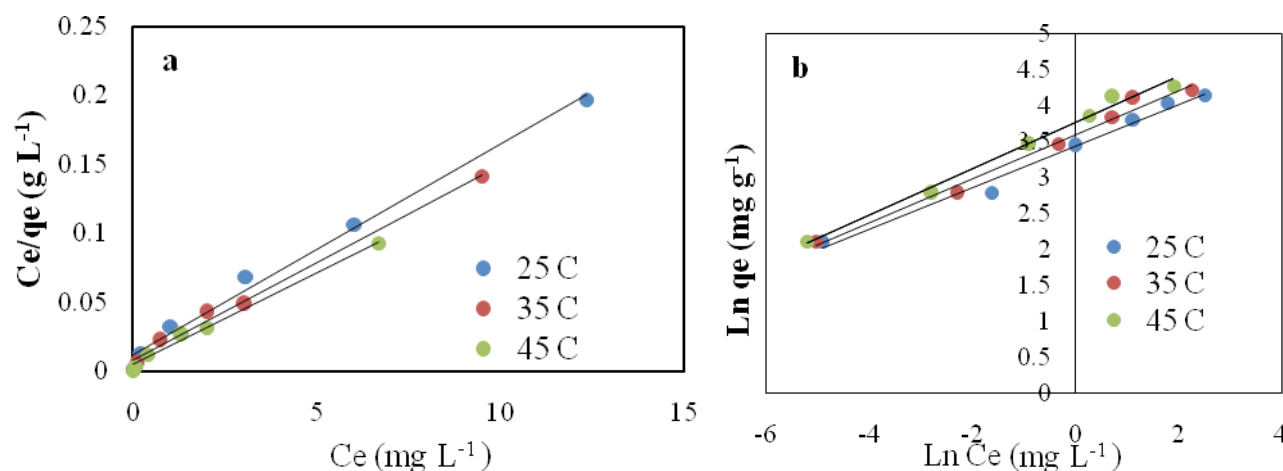| Target	$q_{e,exp}$	Pseudo-first order			Pseudo-second order		
		$q_{e,cal}$ (mg/ g)	K_e (1/min)	R^2	$q_{e,cal}$ (mg/ g)	k_2 (g/(mg min))	R^2
MeP	31.13	20.64	0.059	0.837	32.57	0.1439	0.999

Fig. 8. Langmuir (a) and Freundlich (b) isotherm model of MeP on Fe_3O_4@SiO_2-NH_2 MNPs.

Table 7
Adsorption isotherm parameters and the correlation coefficients for MeP

Isotherm model Temperature	Langmuir			Freundlich		
	q_m (mg/g)	K_1 (L/mg)	R^2	K_f(mg/g) (L/mg)$^{1/n}$	n	R^2
25°C	67.11	0.94	0.99	31.26	3.47	0.98
35°C	70.42	1.92	0.99	32.06	3.26	0.98
45°C	75.2	2.83	0.99	43.67	3.11	0.98

Table 8
Thermodynamic parameters for adsorption of MeP on Fe_3O_4@SiO_2–NH_2

Temperature (°K)	Ln k_c	$\Delta G°$ (kj/mol)	$\Delta H°$ (kj/mol)	$\Delta S°$ (kj/mol K)
293	7.01	–17.08	81.28	0.86
303	7.15	–18.32		
318	7.32	–19.66		

included the standard enthalpy ($\Delta H°$), standard entropy ($\Delta S°$) and standard free energy ($\Delta G°$). The values of the thermodynamic parameters were calculated using the following equations:

$$\ln k_d = \Delta S^o / R - \Delta H^o / RT \tag{8}$$

$$k_d = q_e / C_e \tag{9}$$

$$\Delta G^o = -RT(lnk_d) \tag{10}$$

where T is the temperature (°K); R is the universal gas constant (8.314 J/mol K); K_d is the distribution coefficient (L/g); q_e is the concentration of MeP on the Fe_3O_4@SiO_2-NH_2 MNPs at equilibrium (mg/g) and C_e is the residual MeP concentration in the aqueous phase.

The calculated values of $\Delta H°$, $\Delta G°$, and $\Delta S°$ for the adsorption of MeP on the adsorbent are summarized in Table 8. The negative values of $\Delta G°$ obtained with increasing the temperature confirm the spontaneous nature and practicability of the adsorption process. Whilst, the positive values of $\Delta H°$ reveal that the adsorption of MeP on the adsorbent is endothermic in nature. In addition, the positive values of $\Delta S°$ indicates that the adsorbent has high affinity for MeP adsorption in solid/liquid phase. Similar results were reported by Zhao et al. and Aksu et al. for the

removal of chromium(VI) using Fe_3O_4@SiO_2–NH_2 and the adsorption of 2,4-D by granular activated carbon (GAC) from the aqueous solution, respectively [77,78].

3.8. Reusability studies

To evaluate reusability of the adsorbent, MeP was loaded on the adsorbent (via adsorption process) over five cycles. In each cycle, a 100-ml MeP solution (20 mg/L) was mixed with the adsorbent solution (0.6 g/L) while agitating for 24 h. The adsorbent was separated using an external magnetic field and the supernatant was subjected to MeP measurements. The residual MeP loaded on the adsorbent was mixed with a 50 ml of 0.5 mol/L HNO_3 solution and sonicated for 30 min. The result showed that the adsorption capacity was reduced by 8% in the first cycle followed by ≤ 3.5% for the subsequent four cycles. This demonstrates that the stability of the adsorbent lies within an acceptable criteria concerning the reusability of an adsorbent.

3.9. Comparative study

To highlight the advantages of the adsorbent for the removal of MeP, the results of this work were compared with the other related publications (Table 9). It is clear that the used adsorbent,which is effective and environmentally friendly, could be successfully applied for the removal of micropollutant in water and wastewater treatment. As

Table 9
A comparative study on the MeP removal from aqueous solution

Research number	Removal agent	Removal time	Percentage removal (%)	Reference
1	UV/ TiO_2	240 min	100	[79]
2	$TiO_{2/}$ Fe^{2+}	120 min	100	[80]
3	MNPs-NH_2	30 min	100	[81]
4	MNPs-NH_2	120 min	100	[82]
5	PS/Fe3O4	24 h	19.5	[83]
6	granular activated carbon	168 h	–	[84]
7	MNPs-NH_2 nanoparticles	120 min	98	This work

shown in Table 9, the presented method provided a high removal efficiency compared with others in the literature [79–84].

4. Conclusions

In this study, Fe_3O_4@SiO_2–NH_2 nano-adsorbent was successfully applied for the adsorption and removal of methylparaben from aqueous solutions. The characterization of the adsorbent was carried out by XRD, FTIR, VSM, and SEM, which all confirmed the successful synthesis of the adsorbent. Response surface methodology using the Box–Behnken model was implemented to examine the influential effective operating factors (temperature, adsorbent dosage, time and pH) as well as their interactive effects on the responses in terms of the maximum removal of MeP. It was found out that an increase in the contact time, temperature, and the adsorbent dosage improved the removal efficiency of MeP. The optimization by the model of desirability function revealed that a 98% removal of MeP could be achieved under the optimal conditions. Apparently, the adsorption of MeP on the adsorbent was determined to be endothermic in nature. Adsorption isotherms and kinetic models were well described by the Langmuir and pseudo-first-order model, respectively. Additionally, it was demonstrated that the Box–Behnken model is a well-driven approach to optimize the experiments for the removal of MeP. Finally, the applied amino-functionalized magnetic nanoparticles can be successfully applied for the adsorption and removal of MeP from several aqueous samples.

Acknowledgements

References

[1]   C. Daughton, T. Ternes, Pharmaceuticals& Personal Care Products in the Environment: An Emerging Concern?, Environ. Health. Perspect., 107 (1999) 907–939.

[2]   P. Verlicchi, A. Galletti, M. Petrovic, D. Barceló, Hospital effluents as a source of emerging pollutants: an overview of micropollutants and sustainable treatment options, J. Hydrol., 389 (2010) 416–428.

[3]   D. Błędzka, J. Gromadzińska, W. Wąsowicz, Parabens. From environmental studies to human health, Environ. Int., 67 (2014) 27–42.

[4]   Y.A. Londoño, G.A. Peñuela, Biological removal of different concentrations of ibuprofen and methylparaben in a sequencing batch reactor (SBR), Water. Air. Soil. Pollut., 226 (2015) 1–10.

[5]   Y. Chen, P. Deng, P. Xie, R. Shang, Z. Wang, S. Wang, Heat-activated persulfate oxidation of methyl-and ethyl-parabens: Effect, kinetics, and mechanism, Chemosphere, 168 (2017) 1628–1636.

[6]   M. Soni, I. Carabin, G. Burdock, Safety assessment of esters of p-hydroxybenzoic acid (parabens), Food. Chem. Toxicol., 43 (2005) 985–1015.

[7]   L. Núñez, J. Tadeo, A. García-Valcárcel, E. Turiel, Determination of parabens in environmental solid samples by ultrasonic-assisted extraction and liquid chromatography with triple quadrupole mass spectrometry, J. Chromatogr. A., 1214 (2008) 178–182.

[8]   V. Čiuvašovaitė, E. Adomavičiūtė, V. Vičkačkaitė, Solid-phase microextraction of parabens by polyaniline–polypyrrole coating, Chemija, 18 (2007) 11–15.

[9]   G. Shanmugam, B.R. Ramaswamy, V. Radhakrishnan, H. Tao, GC–MS method for the determination of paraben preservatives in the human breast cancerous tissue, Microchem. J., 96 (2010) 391–396.

[10]   P. Darbre, A. Aljarrah, W. Miller, N. Coldham, M. Sauer, G. Pope, Concentrations of parabens in human breast tumours, J. Appl. Toxicol., 24 (2004) 5–13.

[11]   G.A. Loraine, M.E. Pettigrove, Seasonal variations in concentrations of pharmaceuticals and personal care products in drinking water and reclaimed wastewater in southern California, Environ. Sci. Technol., 40 (2006) 687–695.

[12]   H.-B. Lee, T.E. Peart, M.L. Svoboda, Determination of endocrine-disrupting phenols, acidic pharmaceuticals, and personal-care products in sewage by solid-phase extraction and gas chromatography–mass spectrometry, J. Chromatogr. A., 1094 (2005) 122–129.

[13]   B. Kasprzyk-Hordern, R.M. Dinsdale, A.J. Guwy, The occurrence of pharmaceuticals, personal care products, endocrine disruptors and illicit drugs in surface water in South Wales, UK, Water Res., 42 (2008) 3498–3518.

[14]   M. Terasaki, M. Makino, N. Tatarazako, Acute toxicity of parabens and their chlorinated by-products with Daphnia magna and Vibrio fischeri bioassays, J. Appl. Toxicol., 29 (2009) 242–247.

[15]   M. Terasaki, Y. Takemura, M. Makino, Paraben-chlorinated derivatives in river waters, Environ. Chem. Lett., 10 (2012) 401–406.

[16]   X. Peng, Y. Yu, C. Tang, J. Tan, Q. Huang, Z. Wang, Occurrence of steroid estrogens, endocrine-disrupting phenols, and acid pharmaceutical residues in urban riverine water of the Pearl River Delta, South China, Sci. Total. Environ., 397 (2008) 158–166.

[17]   Y. Yu, Q. Huang, Z. Wang, K. Zhang, C. Tang, J. Cui, J. Feng, X. Peng, Occurrence and behavior of pharmaceuticals, steroid hormones, and endocrine-disrupting personal care products in wastewater and the recipient river water of the Pearl River Delta, South China, J. Environ. Monitor., 13 (2011) 871–878.

[18]   X. Peng, W. Ou, C. Wang, Z. Wang, Q. Huang, J. Jin, J. Tan, Occurrence and ecological potential of pharmaceuticals and personal care products in groundwater and reservoirs in the vicinity of municipal landfills in China, Sci. Total. Environ., 490 (2014) 889–898.

[19]   I. González-Mariño, J.B. Quintana, I. Rodríguez, R. Cela, Evaluation of the occurrence and biodegradation of parabens and halogenated by-products in wastewater by accurate-mass liquid chromatography-quadrupole-time-of-flight-mass spectrometry (LC-QTOF-MS), Water. Res., 45 (2011) 6770–6780.

[20] N. Jonkers, H.-P.E. Kohler, A. Dammshäuser, W. Giger, Mass flows of endocrine disruptors in the Glatt River during varying weather conditions, Environ. Pollu., 157 (2009) 714–723.

[21] S.-M. Lam, J.-C. Sin, A.Z. Abdullah, A.R. Mohamed, Green hydrothermal synthesis of ZnO nanotubes for photocatalytic degradation of methylparaben, Mater. Lett., 93 (2013) 423–426.

[22] J. Sánchez-Martín, J. Beltrán-Heredia, J. Domínguez, Advanced photochemical degradation of emerging pollutants: methylparaben, Water. Air. Soil. Pollut., 224 (2013) 1–12.

[23] K.S. Tay, N.A. Rahman, M.R.B. Abas, Ozonation of parabens in aqueous solution: Kinetics and mechanism of degradation, Chemosphere, 81 (2010) 1446–1453.

[24] D. Dobrin, M. Magureanu, C. Bradu, N. Mandache, P. Ionita, V. Parvulescu, Degradation of methylparaben in water by corona plasma coupled with ozonation, Environ. Sci. Pollu. R., 21 (2014) 12190–12197.

[25] E.M. Cuerda-Correa, J.n.R. Domínguez-Vargas, M.J. Muñoz-Peña, T. González, Ultraviolet-Photoassisted advanced oxidation of parabens catalyzed by hydrogen peroxide and titanium dioxide. Improving the system, Ind. Eng. Chem. R., 55 (2016) 5152–5160.

[26] J. Hu, G. Chen, I.M. Lo, Removal and recovery of Cr (VI) from wastewater by maghemite nanoparticles, Water Res., 39 (2005) 4528–4536.

[27] A.D. Sezer, Recent Advances in Novel Drug Carrier System, InTech, 2012.

[28] T. Neuberger, B. Schöpf, H. Hofmann, M. Hofmann, B. Von Rechenberg, Superparamagnetic nanoparticles for biomedical applications: possibilities and limitations of a new drug delivery system, J. Magn. Magn. Mater., 293 (2005) 483–496.

[29] J.H. Jung, J.H. Lee, S. Shinkai, Functionalized magnetic nanoparticles as chemosensors and adsorbents for toxic metal ions in environmental and biological fields, Chem. Soc. Rev., 40 (2011) 4464–4474.

[30] R. Weissleder, A. Bogdanov, E.A. Neuwelt, M. Papisov, Long-circulating iron oxides for MR imaging, Adv. Drug. Deliver. Rev., 16 (1995) 321–334.

[31] E. Neuwelt, P. Varallyay, A. Bago, L. Muldoon, G. Nesbit, R. Nixon, Imaging of iron oxide nanoparticles by MR and light microscopy in patients with malignant brain tumours, Neuropath. Appl. Neuro., 30 (2004) 456–471.

[32] Y.-X.J. Wang, S.M. Hussain, G.P. Krestin, Superparamagnetic iron oxide contrast agents: physicochemical characteristics and applications in MR imaging, Eur. Radiol., 11 (2001) 2319–2331.

[33] J. Wang, C. Zheng, S. Ding, H. Ma, Y. Ji, Behaviors and mechanisms of tannic acid adsorption on an amino-functionalized magnetic nanoadsorbent, Desalination, 273 (2011) 285–291.

[34] Y.-C. Chang, D.-H. Chen, Preparation and adsorption properties of monodisperse chitosan-bound Fe_3O_4 magnetic nanoparticles for removal of Cu (II) ions, J. Colloid. Interf. Sci., 283 (2005) 446–451.

[35] Y. He, S. Wang, C. Li, Y. Miao, Z. Wu, B. Zou, Synthesis and characterization of functionalized silica-coated Fe_3O_4 superparamagnetic nanocrystals for biological applications, J. Phys. D. Appl. Phys., 38 (2005) 1342.

[36] J. Xu, C. Ju, J. Sheng, F. Wang, Q. Zhang, G. Sun, M. Sun, Synthesis and characterization of magnetic nanoparticles and its application in lipase immobilization, B. Kor. Chem. Soc., 34 (2013) 2408–2412.

[37] V.K. Gupta, A. Fakhri, M. Azad, S. Agarwal, Synthesis of CdSe quantum dots decorated SnO_2 nanotubes as anode for photo-assisted electrochemical degradation of hydrochlorothiazide: Kinetic process, J. Colloid. Interface. Sci., 508 (2017) 575–582.

[38] V.K. Gupta, A. Fakhri, S. Agarwal, M. Azad, Synthesis and characterization of Ag_2S decorated chitosan nanocomposites and chitosan nanofibers for removal of lincosamides antibiotic, Int. J. Biol. Macromolec., 103 (2017) 1–7.

[39] R. Khosravi, A. Azizi, R. Ghaedrahmati, V.K. Gupta, S. Agarwal, Adsorption of gold from cyanide leaching solution onto activated carbon originating from coconut shell—Optimization, kinetics and equilibrium studies, J. Ind. Eng. Chem., 54 (2017) 464–471.

[40] V.K. Gupta, A. Fakhri, S. Rashidi, A.A. Ibrahim, M. Asif, S. Agarwal, Optimization of toxic biological compound adsorption from aqueous solution onto Silicon and Silicon carbide nanoparticles through response surface methodology, Mater. Sci. Eng. C, 77 (2017) 1128–1134.

[41] V.K. Gupta, S. Agarwal, H. Sadegh, G.A.M. Ali, A.K. Bharti, A.S.H. Makhlouf, Facile route synthesis of novel graphene oxide-β-cyclodextrin nanocomposite and its application as adsorbent for removal of toxic bisphenol A from the aqueous phase, J. Mol. Liq., 237 (2017) 466–472.

[42] E. Mäkilä, L.M. Bimbo, M. Kaasalainen, B. Herranz, A.J. Airaksinen, M. Heinonen, E. Kukk, J. Hirvonen, H.l.A. Santos, J. Salonen, Amine modification of thermally carbonized porous silicon with silane coupling chemistry, Langmuir, 28 (2012) 14045–14054.

[43] K. Can, M. Ozmen, M. Ersoz, Immobilization of albumin on aminosilane modified superparamagnetic magnetite nanoparticles and its characterization, Colloid. Surface. B, 71 (2009) 154–159.

[44] A. Subramanian, S.J. Kennel, P.I. Oden, K.B. Jacobson, J. Woodward, M.J. Doktycz, Comparison of techniques for enzyme immobilization on silicon supports, Enzyme. Microb. Tech., 24 (1999) 26–34.

[45] A.H. Lu, E.e.L. Salabas, F. Schüth, Magnetic nanoparticles: synthesis, protection, functionalization, and application, Angew. Chem. Int. Ed., 46 (2007) 1222–1244.

[46] M. Mikhaylova, D.K. Kim, C.C. Berry, A. Zagorodni, M. Toprak, A.S. Curtis, M. Muhammed, BSA immobilization on amine-functionalized superparamagnetic iron oxide nanoparticles, Chem. Mater., 16 (2004) 2344–2354.

[47] D. Loomis, K. Guyton, Y. Grosse, F. El Ghissasi, V. Bouvard, L. Benbrahim-Tallaa, N. Guha, H. Mattock, K. Straif, L. IARC, Carcinogenicity of lindane, DDT, and 2, 4-dichlorophenoxyacetic acid, Lancet. Oncol., 16 (2015) 891.

[48] F.J. Benitez, J.L. Acero, F.J. Real, S. Roman, Oxidation of MCPA and 2, 4-D by UV radiation, ozone, and the combinations UV/H_2O_2 and O_3/H_2O_2, J. Environ. Sci. Health. B, 39 (2004) 393–409.

[49] S. Mangat, P. Elefsiniotis, Biodegradation of the herbicide 2, 4-dichlorophenoxyacetic acid (2, 4-D) in sequencing batch reactors, Water Res., 33 (1999) 861–867.

[50] Y. Liu, Y. Li, X.-M. Li, T. He, Kinetics of (3-aminopropyl) triethoxylsilane (APTES) silanization of superparamagnetic iron oxide nanoparticles, Langmuir, 29 (2013) 15275–15282.

[51] X. Yi, W. Shi, S. Yu, Y. Wang, N. Sun, L. Jin, S. Wang, Isotherm and kinetic behavior of adsorption of anion polyacrylamide (APAM) from aqueous solution using two kinds of PVDF UF membranes, J. Hazard. Mater., 189 (2011) 495–501.

[52] Y. Xue, H. Hou, S. Zhu, Adsorption removal of reactive dyes from aqueous solution by modified basic oxygen furnace slag: isotherm and kinetic study, Chem. Eng. J., 147 (2009) 272–279.

[53] B. Kakavandi, A. Jonidi, R. Rezaei, S. Nasseri, A. Ameri, A. Esrafily, Synthesis and properties of Fe_3O_4-activated carbon magnetic nanoparticles for removal of aniline from aqueous solution: equilibrium, kinetic and thermodynamic studies, Iran. J. Environ. Health. Sci. Engin., 10 (2013) 19.

[54] A.A. Babaei, A. Khataee, E. Ahmadpour, M. Sheydaei, B. Kakavandi, Z. Alaee, Optimization of cationic dye adsorption on activated spent tea: Equilibrium, kinetics, thermodynamic and artificial neural network modeling, Kor. J. Chem. Engin., 33 (2016) 1352–1361.

[55] F.J. Beltrán, P. Pocostales, P. Alvarez, A. Oropesa, Diclofenac removal from water with ozone and activated carbon, J. Hazard. Mater., 163 (2009) 768–776.

[56] R.F. Gunst, Response Surface Methodology: Process and Product Optimization Using Designed Experiments, in, Taylor & Francis Group. 1996.

[57] K. Yetilmezsoy, S. Demirel, R.J. Vanderbei, Response surface modeling of Pb (II) removal from aqueous solution by Pistacia vera L.: Box–Behnken experimental design, J. Hazard. Mater., 171 (2009) 551–562.

[58] R. Ragonese, M. Macka, J. Hughes, P. Petocz, The use of the Box–Behnken experimental design in the optimisation and robustness testing of a capillary electrophoresis method for the analysis of ethambutol hydrochloride in a pharmaceutical formulation, J. Pharmaceutic. Biomed., 27 (2002) 995–1007.

[59] G. Annadurai, R. Sheeja, Use of Box-Behnken design of experiments for the adsorption of verofix red using biopolymer, Bioprocess. Biosyst. Eng., 18 (1998) 463–466.

[60] A. Kumar, B. Prasad, I. Mishra, Optimization of process parameters for acrylonitrile removal by a low-cost adsorbent using Box–Behnken design, J. Hazard. Mater., 150 (2008) 174–182.

[61] T. Yang, C. Shen, Z. Li, H. Zhang, C. Xiao, S. Chen, Z. Xu, D. Shi, J. Li, H. Gao, Highly ordered self-assembly with large area of Fe_3O_4 nanoparticles and the magnetic properties, J. Phys. Chem. B, 109 (2005) 23233–23236.

[62] M. Yamaura, R. Camilo, L. Sampaio, M. Macedo, M. Nakamura, H. Toma, Preparation and characterization of (3-aminopropyl) triethoxysilane-coated magnetite nanoparticles, J. Magn. Magn. Mater., 279 (2004) 210–217.

[63] M. Behbahani, S. Bagheri, M.M. Amini, H. Sadeghi, Abandansari, H.R. Moazami, A. Bagheri, Application of a magnetic molecularly imprinted polymer for the selective extraction and trace detection of lamotrigine in urine and plasma samples, J. Sep. Sci., 37 (2014) 1610–1616.

[64] M. Ghambarian, M. Behbahani, A. Esrafili, H.R. Sobhi, Application of a dispersive solid-phase extraction method using an amino-based silica-coated nanomagnetic sorbent for the trace quantification of chlorophenoxyacetic acids in water samples, J. Sep. Sci., 40 (2017) 3479–3486.

[65] J. Safari, Z. Zarnegar, Ultrasonic activated efficient synthesis of chromenes using amino-silane modified Fe_3O_4 nanoparticles: a versatile integration of high catalytic activity and facile recovery, J. Mol. Struct., 1072 (2014) 53–60.

[66] R. Bhaumik, N.K. Mondal, S. Chattoraj, J.K. Datta, Application of response surface methodology for optimization of fluoride removal mechanism by newly developed biomaterial, Am. J. Analyt. Chem., 4 (2013) 404.

[67] P. Tripathi, V.C. Srivastava, A. Kumar, Optimization of an azo dye batch adsorption parameters using Box–Behnken design, Desalination, 249 (2009) 1273–1279.

[68] D. Liu, Z. Li, W. Li, Z. Zhong, J. Xu, J. Ren, Z. Ma, Adsorption behavior of heavy metal ions from aqueous solution by soy protein hollow microspheres, Ind. Eng. Chem. Res., 52 (2013) 11036–11044.

[69] M. Meng, Z. Wang, L. Ma, M. Zhang, J. Wang, X. Dai, Y. Yan, Selective adsorption of methylparaben by submicrosized molecularly imprinted polymer: batch and dynamic flow mode studies, Ind. Eng. Chem. Res., 51 (2012) 14915–14924.

[70] M. Mahdavi, M.B. Ahmad, M.J. Haron, Y. Gharayebi, K. Shameli, B. Nadi, Fabrication and characterization of SiO_2/(3-aminopropyl) triethoxysilane-coated magnetite nanoparticles for lead (II) removal from aqueous solution, J. Inorg. Organomet. Polym. Mater., 23 (2013) 599–607.

[71] M. Anbia, M. Lashgari, Synthesis of amino-modified ordered mesoporous silica as a new nano sorbent for the removal of chlorophenols from aqueous media, Chem. Engin. J., 150 (2009) 555–560.

[72] J. Wang, S. Zheng, Y. Shao, J. Liu, Z. Xu, D. Zhu, Amino-functionalized $Fe_3O_4@SiO_2$ core–shell magnetic nanomaterial as a novel adsorbent for aqueous heavy metals removal, J. Colloid. Interface. Sci., 349 (2010) 293–299.

[73] H. Barndõk, D. Hermosilla, C. Han, D.D. Dionysiou, C. Negro, Á. Blanco, Degradation of 1, 4-dioxane from industrial wastewater by solar photocatalysis using immobilized NF-TiO_2 composite with monodisperse TiO_2 nanoparticles, Appl. Catal. B, 180 (2016) 44–52.

[74] R. Tabaraki, S. Ahmady-Asbchin, O. Abdi, Biosorption of Zn(II) from aqueous solutions by Acinetobacter sp. isolated from petroleum spilled soil, J. Environ. Chem. Engin., 1 (2013) 604–608.

[75] U. Guyo, J. Mhonyera, M. Moyo, Pb(II) adsorption from aqueous solutions by raw and treated biomass of maize stover – A comparative study, Process. Saf. Environ., 93 (2015) 192–200.

[76] J. Zhang, S. Zhai, S. Li, Z. Xiao, Y. Song, Q. An, G. Tian, Pb (II) removal of $Fe_3O_4@SiO_2$–NH_2 core–shell nanomaterials prepared via a controllable sol–gel process, Chem. Engin. J., 215 (2013) 461–471.

[77] Y.-G. Zhao, H.-Y. Shen, S.-D. Pan, M.-Q. Hu, Q.-H. Xia, Preparation and characterization of amino-functionalized nano-Fe_3O_4 magnetic polymer adsorbents for removal of chromium (VI) ions, J. Mater. Sci., 45 (2010) 5291–5301.

[78] Z. Aksu, E. Kabasakal, Batch adsorption of 2, 4-dichlorophenoxy-acetic acid (2, 4-D) from aqueous solution by granular activated carbon, Sep. Purif. Technol., 35 (2004) 223–240.

[79] T. Velegraki, E. Hapeshi, D. Fatta-Kassinos, I. Poulios, Solar-induced heterogeneous photocatalytic degradation of methyl-paraben, Appl. Catal. B., 178 (2015) 2–11.

[80] H. Zúñiga-Benítez, C. Aristizábal-Ciro, G.A. Peñuela, Photodegradation of the endocrine-disrupting chemicals benzophenone-3 and methylparaben using Fenton reagent: optimization of factors and mineralization/biodegradability studies, J. Taiwan. Inst. Chem. Eng., 59 (2016) 380–388.

[81] J. Zhang, S. Zhai, S. Li, Z. Xiao, Y. Song, Q. An, G. Tian, Pb (II) removal of $Fe_3O_4@SiO_2$–NH_2 core–shell nanomaterials prepared via a controllable sol–gel process, Chem. Eng. J., 215 (2013) 461–471.

[82] J. Wang, C. Zheng, S. Ding, H. Ma, Y. Ji, Behaviors and mechanisms of tannic acid adsorption on an amino-functionalized magnetic nanoadsorbent, Desalination, 273 (2011) 285–291.

[83] H.W. Chen, C.S. Chiou, S.H. Chang, Comparison of methylparaben, ethylparaben and propylparaben adsorption onto magnetic nanoparticles with phenyl group, Powder Technol., 311 (2017) 426–431.

[84] N.Y. Delgado, A.L. Capparelli, D.J. Marino, A.F. Navarro, G.A. Peñuela, A.E. Ronco, Adsorption of pharmaceuticals and personal care products on granular activated carbon, J. Surf. Eng. Mater. Adv. Technol., 6(2016) 183–200.